Chinese Journal of Catalysis 39 (2018) 1711–1723

available at www.sciencedirect.com

ScienceDirect

journal homepage: www.elsevier.com/locate/chnjc

Article

Selective hydrogenolysis of furfuryl alcohol to 1,5- and 1,2-pentanediol over Cu-$LaCoO_3$ catalysts with balanced Cu^0-CoO sites

Fangfang Gao [a,b], Hailong Liu [a], Xun Hu [a], Jing Chen [a,#], Zhiwei Huang [a,*], Chungu Xia [a]

[a] *State Key Laboratory for Oxo Synthesis and Selective Oxidation, Suzhou Research Institute of LICP, Lanzhou Institute of Chemical Physics (LICP), Chinese Academy of Sciences, Lanzhou 730000, Gansu, China*

[b] *University of Chinese Academy of Sciences, Beijing 100049, China*

ARTICLE INFO

Article history:
Received 7 April 2018
Accepted 25 May 2018
Published 5 October 2018

Keywords:
Furfuryl alcohol
Selective hydrogenolysis
Pentanediol
Cu-$LaCoO_3$ catalyst
Perovskite structure

ABSTRACT

Selective hydrogenolysis of biomass-derived furfuryl alcohol (FFA) to 1,5- and 1,2-pentanediol (PeD) was conducted over Cu-$LaCoO_3$ catalysts with different Cu loadings; the catalysts were derived from perovskite structures prepared by a one-step citrate complexing method. The catalytic performances of the Cu-$LaCoO_3$ catalysts were found to depend on the Cu loading and pretreatment conditions. The catalyst with 10 wt% Cu loading exhibited the best catalytic performance after prereduction in 5%H_2-95%N_2, achieving a high FFA conversion of 100% and selectivity of 55.5% for 1,5-pentanediol (40.3%) and 1,2-pentanediol (15.2%) at 413 K and 6 MPa H_2. This catalyst could be reused four times without a loss of FFA conversion but it resulted in a slight decrease in pentanediol selectivity. Correlation between the structural changes in the catalysts at different states and the simultaneous variation in the catalytic performance revealed that cooperative catalysis between Cu^0 and CoO promoted the hydrogenolysis of FFA to PeDs, especially to 1,5-PeD, while Co^0 promoted the hydrogenation of FFA to tetrahydrofurfuryl alcohol (THFA). Therefore, it is suggested that a synergetic effect between balanced Cu^0 and CoO sites plays a critical role in achieving a high yield of PeDs with a high 1,5-/1,2-pentanediol selectivity ratio during FFA hydrogenolysis.

1. Introduction

The conversion of renewable and abundant biomass feedstock available in nature into chemicals and fuels is considered a feasible technique to alleviate the current increasing environmental and resource problems [1–3]. Furfural (FA) is an important platform chemical, industrially produced from lignocellulosic biomass through acidic hydrolysis. It can be converted into a variety of important chemicals and fuels, such as 1,2-pentanediol (1,2-PeD), 1,5-pentanediol (1,5-PeD), furan, 2-methyl furan, cyclopentanone, and γ-valerolactone [4–7]. Particularly, the selective hydrogenolysis of FA and its derivatives, furfuryl alcohol (FFA) and tetrahydrofurfuryl alcohol (THFA), into useful diols, such as 1,2-PeD and 1,5-PeD, is noticeably attractive [8–12]. These PeDs are widely used for the production of microbicides, cosmetics, polyesters, plastics, etc.

* Corresponding author. Tel: +86-931-4968070; Fax: +86-931-4968129; E-mail: zwhuang@licp.cas.cn
# Corresponding author. Tel: +86-931-4968068; Fax: +86-931-4968129; E-mail: chenj@licp.cas.cn

This work was supported by the National Natural Science Foundation of China (21473224), Key Research Project of Frontier Science of Chinese Academy of Sciences (QYZDJ-SSW-SLH051), the Youth Innovation Promotion Association, CAS (2016371), and the Suzhou Science and Technology Development Plan (SYG201626).
DOI: 10.1016/S1872-2067(18)63110-9 | http://www.sciencedirect.com/science/journal/18722067 | Chin. J. Catal., Vol. 39, No. 10, October 2018

[6,13]. Nowadays, PeDs are generally produced via a cost-intensive multistep route from petroleum-derived feedstocks involving selective oxidation and reduction reactions [9,13]. The availability of FA from abundant renewable lignocellulose [3], in contrast to non-renewable C_5 petroleum feedstocks, makes the selective hydrogenolysis of FA and its derivatives of FFA/THFA a practical pathway for the sustainable production of PeDs with high energy efficiency.

Thus far, the selective hydrogenolysis of FA or its derivatives at the C–O bonds in the furan ring to produce PeDs mainly focused on using supported catalysts of group VIII precious metals (Ru [13], Pt [12,14,15], Rh [16–21], and Ir [22–26]). Low-valency metallic oxides (such as ReO_x, MoO_x, VO_x or WO_x)-incorporated Rh [16,18,19,21] and Ir [22–24,26] catalysts attracted much attention for the hydrogenolysis of THFA to synthesize 1,5-PeD. Tomishige's group [19–25] led pioneering work on such reactions and achieved a high 1,5-PeD yield of 94.0% at 373 to 393 K and 8 MPa H_2. Further, basic supports, such as MnO_x, CeO_2, and hydrotalcite (HT)-supported noble metals of Ru [13] and Pt [12,14] were applied to convert FA/FFA to 1,2-PeD at 423–443 K and 1–2 MPa H_2; 1,2-PeD with a yield of up to 80% was achieved over a Pt/HT catalyst at a high Pt to FFA molar ratio of 1/1. In addition, there are a few reports on the use of non-precious metals, such as Cu [8,27–29], Co [10,30], and Ni-based [11,31] catalysts in the hydrogenolysis of FFA and THFA to PeDs. Generally, Cu-based catalysts exhibit higher selectivity toward 1,2-PeD, while Co and Ni-based catalysts prefer the generation of 1,5-PeD. For instance, Cu-$Mg_3AlO_{4.5}$ [8] with a basic support hydrogenolyzed FFA to 1,2-PeD and 1,5-PeD with yields of 51.2% and 28.8%, respectively, at 413 K and 6 MPa H_2, while a Ni-Y_2O_3 [11] composite catalyst selectively hydrogenolyzed FFA to 1,5-PeD (41.9%) rather than 1,2-PeD (1.2%) at 423 K and 2 MPa H_2. Clearly, studies on FA and its derivatives subjected to hydrogenolysis still encounter low activities or selectivities toward target PeDs, or the use of noble metal catalysts. It is thus urgent to develop effective and environmentally benign non-precious metal catalysts for the efficient conversion of FA and its derivatives into value-added PeDs. However, the development of effective methods for tuning the chemoselectivity of FA and its derivatives for hydrogenolysis is a great challenge at present.

Recently, owing to the flexibility of their electronic and crystal structure as well as their chemical versatility, perovskite-type oxides with a general ABO_3 structure have been studied for catalysis applications [32–37]. Using perovskite-type oxides as precursors to stabilize metal particles on mixed oxides is also an attractive option to produce active and stable catalysts [32,33]. In addition, the specific surface acidity/basicity of perovskite-type oxides also contributes to the novel performance of the catalysts [36,37]. Taking these advantages of perovskite-based catalysts and the high C–O hydrogenation/hydrogenolysis activity of the non-noble metal Cu [8,38,39] into consideration, a series of Cu-$LaCoO_3$ perovskite-type mixed oxides with different Cu loadings were synthesized in the current study and investigated for the selective hydrogenolysis of FFA to value-added PeDs. The Cu-$LaCoO_3$ catalysts were found to exhibit a higher selectivity for 1,5-PeD over 1,2-PeD, with a 1,5-PeD/1,2-PeD selectivity ratio of up to 3/1; this result is much higher than that obtained in previous studies on Cu-based catalysts, such as copper chromite (3/4) [29], Cu-$Mg_3AlO_{4.5}$ (3/5) [8], and Cu-Al_2O_3 (1/2.2) [27]. The possible reasons for the higher selectivity of Cu-$LaCoO_3$ catalysts towards 1,5-PeD are discussed in terms of the effect of different reduction atmospheres and the catalysts characterized at different states are.

2. Experimental

2.1. Materials

All the reagents were of analytical grade and directly used without further pretreatment. $H_2PtCl_6{\cdot}6H_2O$ and $RuCl_3{\cdot}3H_2O$ were purchased from Shaanxi Rock New Materials Co., Ltd., China. $PdCl_2$ and $RhCl_3{\cdot}3H_2O$ were purchased from Beijing HWRK Chem Co., Ltd., China. $CuCr_2O_4$ catalyst was purchased from Yingkou Tianyuan Chemical Industry Research Institute Co., Ltd., China. FFA and THFA were purchased from Alfa Aesar. 5%H_2-95%Ar, 5%H_2-95%N_2, H_2 (99.999%), and He (99.999%) were obtained from Lanzhou Lanmei Cryogenic Products Co., Ltd., China. CO_2 (99.99%) was obtained from Lanzhou Hongli gas Co., Ltd., China.

2.2. Catalyst preparation

In this study, a series of xCuO-$LaCoO_3$ (x/% = 0, 2, 5, 10, 15, and 20) perovskite-type mixed oxides were synthesized by the citric-complexing method [32]. The desired amounts of copper, cobalt, and lanthanum nitrates with a La/Co molar ratio of 1/1 were dissolved in deionized (DI) water at a concentration of Cu^{2+} = 0.1 mol/L. Later, citric acid (20% excess over the total molar content of metal cations) and polyethylene glycol 400 (24% molar amount of citric acid) were added to the solution. The solution was stirred at room temperature for 6 h and then stirred at 353 K until a foamy solid was formed. The foamy solid was dried at 383 K for 12 h and then calcined at 973 K for 2 h in static air with a temperature ramping rate of 3 K/min. The calcined samples were marked as xCuO-$LaCoO_3$, where x represents the nominal Cu loading. The corresponding reduced catalysts were labeled as xCu-$LaCoO_3$. $LaCoO_3$-supported Pt, Ru, Pd, and Rh catalysts with individual nominal loading of 5 wt% were also prepared by a similar method.

2.3. Catalyst characterization

X-ray diffraction (XRD) experiments were performed on a PANalytical X'pert Pro Diffractometer with nickel-filtered Cu K_α radiation (λ = 1.05406 nm) at 40 kV and 40 mA. The patterns were collected in the 2θ range of 10°–80° at a scanning speed of 10°/min.

The Brunauer-Emmett-Teller (BET) surface area of the catalysts was determined using the N_2 adsorption-desorption method and the experiments were conducted on a Micromeritics Tristar II 3020 instrument at liquid nitrogen temperatures (77 K). Prior to these measurements, the samples were pre-

treated with N_2 at 363 K for 2 h and then maintained for 4 h at 573 K.

The reducibility and surface acidity/basicity of the calcined samples were determined by H_2-temperature-programmed reduction (TPR) and NH_3/CO_2-Temperature programmed desorption (TPD) measurements, respectively, with a DAX-7000 instrument (Huasi Technology Co., Ltd, China). For H_2-TPR experiments, ~50 mg of the samples was placed in a quartz cell and pretreated at 473 K under He flow for 1 h. After cooling to 303 K, the samples were reduced in 5%H_2-95%Ar flow (40 mL/min) and the temperature was increased linearly to 1073 K at a ramping rate of 10 K/min. H_2 consumption was monitored by thermal conductivity detector (TCD). For CO_2-TPD experiments, ~0.2 g of the samples was placed in a quartz cell and pretreated at 473 K under He flow for 1 h and then reduced at 573 K in 5%H_2-95%Ar flow (40 mL/min) for 2 h. After cooling to 313 K, the samples were exposed to CO_2 flow (40 mL/min) and maintained for 1 h. Subsequently, the temperature was increased linearly to 1173 K at a ramping rate of 5 K/min under He flow; the desorbed CO_2 was monitored by TCD. NH_3-TPD of the 10 wt% Cu-$LaCoO_3$ catalyst was similar to the CO_2-TPD procedure above but with the saturation adsorption of NH_3 at 373 K for 1 h.

Transmission electron microscopy (TEM) tests were performed on a TECNAI G2 TF20 instrument at 200 kV. The TEM samples were prepared by ultrasonic dispersion in ethanol. After ultrasonic dispersion of the catalysts, the samples were deposited on copper grids with a porous carbon film support.

X-ray photoelectron spectra (XPS) measurements were carried out on an ESCALAB250xi spectrometer equipped with an Al K_α X-ray radiation source ($h\upsilon$ = 1486.6 eV). The sample binding energy can be calibrated with C 1*s* (E_b = 284.8 eV) peak as the internal standard, the error is about ± 0.2.

The chemical composition of the catalysts was determined by X-ray fluorescence (XRF) on a PANalytical MagixPW2403 instrument.

Carbon deposition and stability of the used catalysts were determined on a NETZSCH STA449F3 thermogravimetry-differential scanning calorimetry (TG-DSC) instrument. Initially, 10 mg of the samples were placed in an alumina crucible and heated to 1073 K at a heating rate of 10 K/min in a nitrogen atmosphere.

2.4. Catalytic hydrogenolysis of furfuryl alcohol

The selective hydrogenolysis of FFA was carried out in a 100 mL stainless steel autoclave at a stirring speed of 800 r/min. All the calcined samples were used in the powder form. Prior to each test, the calcined samples with a granule size of 60–80 mesh were pre-reduced in 5%H_2-95%N_2 flow (40 mL/min) at 573 K for 3 h. In a typical run, 30 g of 5 wt% FFA in ethanol solution together with the pre-reduced catalyst were introduced into the autoclave. After purging thrice with H_2, the reactor was pressurized to 6 MPa and heated to 413 K to start the reaction. For comparison, the hydrogenolysis of THFA was also studied over the 10Cu-$LaCoO_3$ catalyst using similar conditions.

After centrifugation, the products were identified using an Agilent 7890A/5975C gas chromatograph-mass spectrometer (GC-MS) with an HP-5MS column. The reactant and liquid products were analyzed by gas chromatography (Agilent 7890A GC) with a PONA capillary column (50 m × 0.20 mm × 0.50 μm) and a flame ionization detector (FID). Conversion and product selectivity were determined by an internal standard method and calculated as follows:

$$\text{Conversion}(\%) = \frac{\text{initial moles of FFA} - \text{moles of FFA left}}{\text{initial moles of FFA}} \times 100\%$$

$$\text{Selectivity}(\%) = \frac{\text{moles of a product generated}}{\text{initial moles of FFA} - \text{moles of FFA left}} \times 100\%$$

3. Results and discussion

3.1. Structural characterization of Cu-$LaCoO_3$ catalysts

Fig. 1 shows the XRD patterns of calcined *x*CuO-$LaCoO_3$ samples with different Cu loadings. Strong peaks due to the formation of $LaCoO_3$ perovskite-type oxides were seen in the pattern of the $LaCoO_3$ support. Additionally, segregated phases due to the formation of $La_2O_2CO_3$ (diffraction peaks at 22.3°, 25.8°, 30.4°, 44.4°, and 47.4°) and Co_3O_4 (at 36.8 °) were also observed. $La_2O_2CO_3$ was probably formed by CO_2-induced decomposition of $LaCoO_3$ to La_2O_3 and Co_3O_4 and the further reaction of La_2O_3 and CO_2 in air during the calcination process [33]. The incorporation of Cu, even at an amount as small as 2 wt%, resulted in the decomposition of the $LaCoO_3$ perovskite

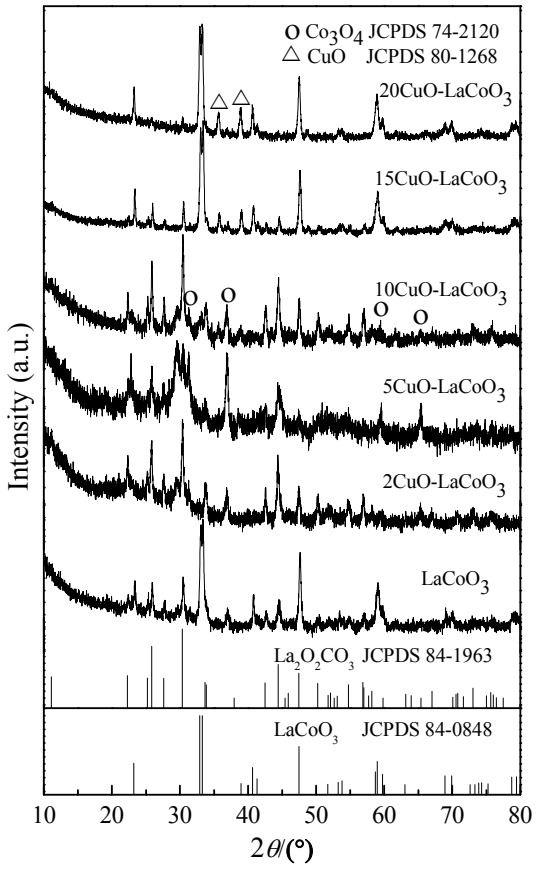

Fig. 1. XRD patterns of calcined *x*CuO-$LaCoO_3$ catalysts with different Cu loadings.

structure to $La_2O_2CO_3$ and Co_3O_4 and almost no diffraction peaks associated with the $LaCoO_3$ perovskite could be observed at 5 wt% Cu. Furthermore, the diffraction peaks of Co_3O_4 further intensified in the pattern of 5CuO-$LaCoO_3$. No clear diffraction peaks corresponding to CuO could be seen in the samples with Cu loading below 5 wt%, which is probably due to the high dispersion of Cu in these samples. Increasing the Cu loading to 10 wt% led to the appearance of diffraction peaks corresponding not only to the $LaCoO_3$ perovskite, but also CuO, with a simultaneous decrease in the Co_3O_4 diffraction peaks. The peaks of the $LaCoO_3$ perovskite and CuO further intensified with an increase in the Cu loading to 20 wt%, while the peaks assignable to Co_3O_4 almost disappeared in the pattern of 20CuO-$LaCoO_3$. It seems that the incorporation of small amounts ((2–10) wt%) of Cu caused the segregation of $LaCoO_3$, which is similar to the effect observed when Zn was incorporated in $LaCoO_3$ [40]. The gradual increase in the intensity of CuO peaks with an increase in the Cu loading could be ascribed to the aggregation of CuO particles.

Fig. 2 presents the XRD patterns of 10Cu-$LaCoO_3$ samples at different states. After reduction in pure H_2 at 573 K, the diffraction peaks of CuO disappeared; meanwhile, the diffraction peaks corresponding to cubic Cu^0 (PDF#04-0836) appeared (Fig. 2(2)), suggesting that CuO in the sample was reduced to Cu^0. The disappearance of Co_3O_4 diffraction peaks suggests that Co_3O_4 was reduced to Co species with low valencies, i.e., Co^0 and/or CoO. Nonetheless, no diffraction peaks associated with Co^0 or CoO could be observed, which is probably due to the high dispersion of these species. After reduction in 5%H_2-95%N_2 at the same temperature, however, almost no diffraction peaks associated with Cu^0 and/or Cu_2O were observed (Fig. 2(3)), while the diffraction peaks of CuO (PDF#80-1268) and Co_3O_4 (PDF#74-2120) still remained, showing that the catalyst was hardly reduced under these conditions. These findings also suggest that the catalyst exhibited a high reducibility in pure H_2. As for the catalyst reduced in 5%H_2-95%N_2 and used for one time, the diffraction peaks of Cu^0 appeared in its XRD pattern; no CuO could be observed and the intensity of the diffraction peaks of Co_3O_4 decreased (Fig. 2(4)), indicating that CuO was reduced to Cu^0 and Co_3O_4 was largely reduced to Co^0 and/or CoO with high dispersion. This finding also suggests that the reaction media of FFA in alcohol has a stronger reducibility than 5%H_2-95%N_2 at 573 K. The diffraction peaks of Co_3O_4 almost disappeared after the catalyst was used for 4 cycles (Fig. 2(5)), indicating that Co_3O_4 was continuously reduced to Co^0 and/or CoO during the repeat reactions. The reduction of CoO, which is more difficult to be reduced than Co_3O_4 [10,41], is also observed during glycerol hydrogenolysis [41]. The intensity of the diffraction peaks of Cu^0 as well as those of $La_2O_2CO_3$ (Fig. 2(5)) decreased after the catalyst was used four times. Such obvious structural changes in the catalyst during repeated runs may be related to the changes in its catalytic performance, as will be discussed later.

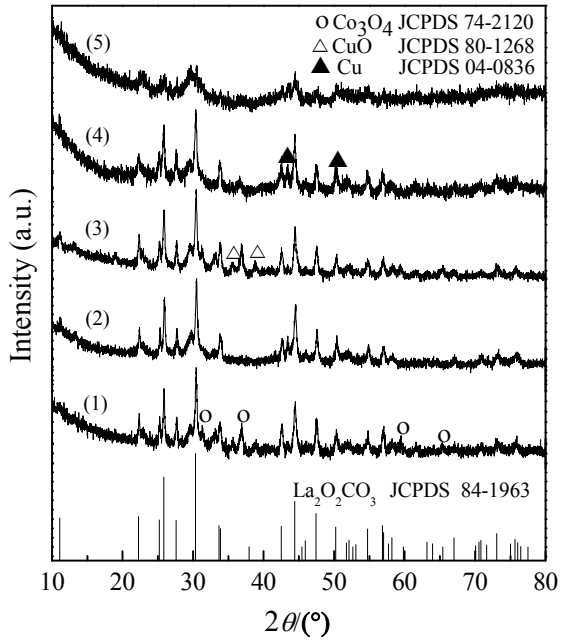

Fig. 2. XRD patterns of 10Cu-$LaCoO_3$ catalysts at different states. (1) calcined, (2) reduced in pure H_2, (3) reduced in 5%H_2-95%N_2, (4) reduced in 5%H_2-95%N_2 and used once, and (5) reduced in 5%H_2-95%N_2 and used four times.

Fig. 3 shows the XPS survey of the Cu and Co species. As can be seen in Fig. 3(a), the binding energy of Cu $2p_{3/2}$ at 933.5 eV along with a satellite peak in the range of 940–945 eV indicate the existence of Cu^{2+} in the calcined sample [42]. The decrease in the binding energy of Cu $2p_{3/2}$ to 932.5 eV and the weakening or even disappearance of the satellite peak suggests that Cu species were reduced to Cu with low valencies (Cu^0 or Cu_2O) in both reduced samples as well as the samples used for one time. The simulation of Cu 2*p* (Fig. 3(a)–(2)) for the reduced catalyst confirmed the coexistence of large amounts of Cu species with low valencies. The decrease in the intensity of the Cu 2*p* spectra with a high binding energy corresponding to the used catalyst indicated a decrease in the Cu^{2+} amount [42]. As for the Co 2*p* spectrum of the calcined sample, the asymmetric peak at 780.5 eV corresponding to Co $2p_{3/2}$ and the presence of a weak peak of Co $2p_{1/2}$ at about 796.6 eV are characteristic of Co^{3+} [43]. The peaks of Co $2p_{3/2}$ at 782.3 eV and the weak peak at 798.5 eV were associated with Co^{2+}. The simulation of Co 2*p* ((b)–(2)) for the reduced catalyst confirmed the coexistence of Co^{3+} and Co^{2+} species [43]. From Fig. 3(b), we can see that after being used once, the Co 2*p* signal weakened (Fig. 3(b)–(3)) and exhibited a tendency to shift towards lower binding energies, indicating an increase in low-state Co species. These findings are in line with the results of XRD characterization shown in Fig. 2.

Fig. 4 shows the TEM images of calcined CuO-$LaCoO_3$ samples with Cu loadings of (2, 10, and 20) wt% as well as those of reduced and used 10Cu-$LaCoO_3$ catalysts. The calcined samples generally exhibited an amorphous structure, which is in line with previous findings by Predoana et al. [44]. It is difficult to discriminate between CuO nanoparticles and the $LaCoO_3$ support when the Cu loading was low (i.e., 2 wt%), which indicates the uniform dispersion of CuO. With further increase in Cu loading, a small amount of aggregated particles with sizes around 5–10 nm were observed in 10CuO-$LaCoO_3$ and the aggregated particles became more obvious when the Cu loading was 20 wt%. Such aggregation could be ascribed to CuO, as

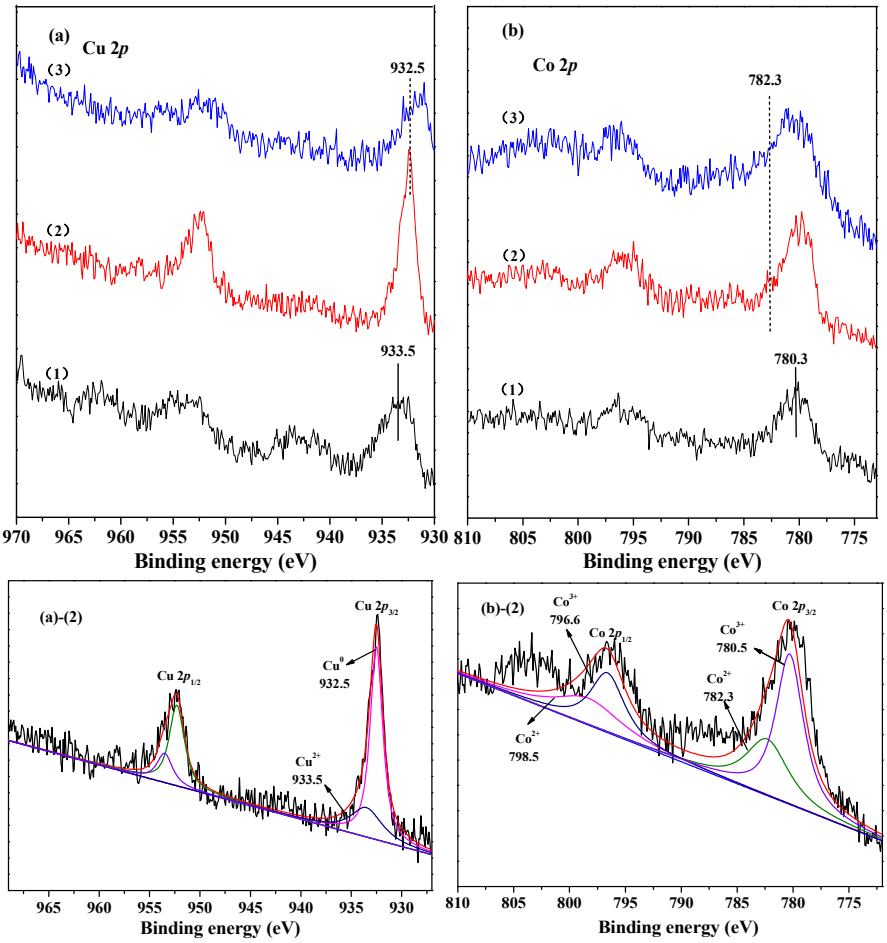

Fig. 3. XPS spectra for Cu 2*p* (a) and Co 2*p* (b) of (1) calcined 10CuO-$LaCoO_3$ samples, (2) reduced 10Cu-$LaCoO_3$ samples in 5%H_2-95%N_2, and (3) reduced 10Cu-$LaCoO_3$ samples in 5%H_2-95%N_2 and used once.

evidenced from XRD characterization (Fig. 1). There was no obvious change in the morphology of the 10Cu-$LaCoO_3$ catalyst after reduction in 5%H_2-95%N_2 at 573 K (Fig. 4(d)). High resolution transmission electron microscope (HRTEM) images and Energy dispersive spectrdmeter (EDS) mapping analysis of the reduced 10Cu-$LaCoO_3$ catalyst indicate that Cu, Co, and La were distributed quite evenly and $La_2O_2CO_3$, $LaCoO_3$ and Co_3O_4 coexisted in the catalyst; these observations are consistent with the XRD results. However, a number of dark particles could be clearly seen when the catalyst was used four times. These dark particles may be associated with the continuous sintering of Cu^0 particles during the reaction process. Note that the deposited carbon due to coke formation can also cause the particles in the used catalyst to appear a little bit darker. The formation of coke in the used catalyst was supported by a clear mass loss in the TG profile in the range of 550–855 K, as will be shown later.

The reducibility of the calcined samples was studied by TPR (Fig. 5). It can be seen that the $LaCoO_3$ support was reduced in two major regions. The first one in the range of 644–890 K and centered at about 763 K might be associated with the reduction of Co^{3+} to Co^{2+} and the second one at temperatures above 890 K might be attributed to the reduction of Co^{2+} owing to interactions with La^{3+} species to Co^0 [45]. An obvious shift in the re-

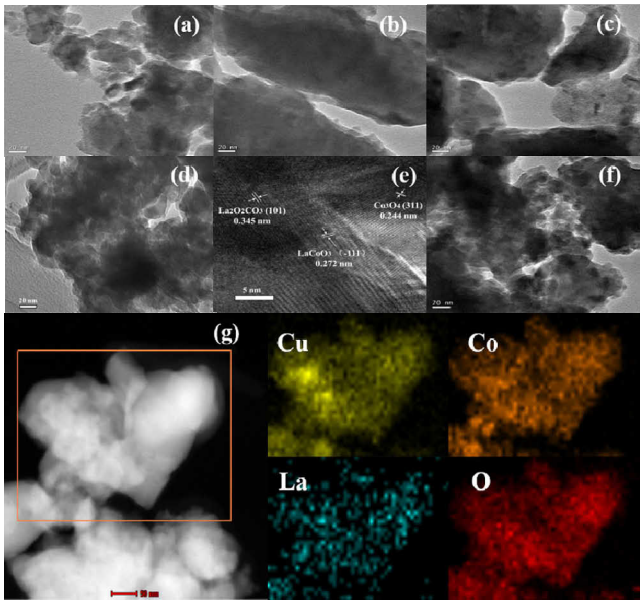

Fig. 4. TEM and HRTEM images of (a) calcined 2CuO-$LaCoO_3$, (b) calcined 10CuO-$LaCoO_3$, (c) calcined 20CuO-$LaCoO_3$, (d, e) reduced 10Cu-$LaCoO_3$ in 5%H_2-95%N_2, and (f) 10Cu-$LaCoO_3$ used four times; (g) High-angle Annular Dark Field-scanning transmission electron microscope (HAADF-STEM) image of 10Cu-$LaCoO_3$ reduced in 5%H_2-95%N_2, and the corresponding EDS elemental mappings of Cu, Co, La, and O.

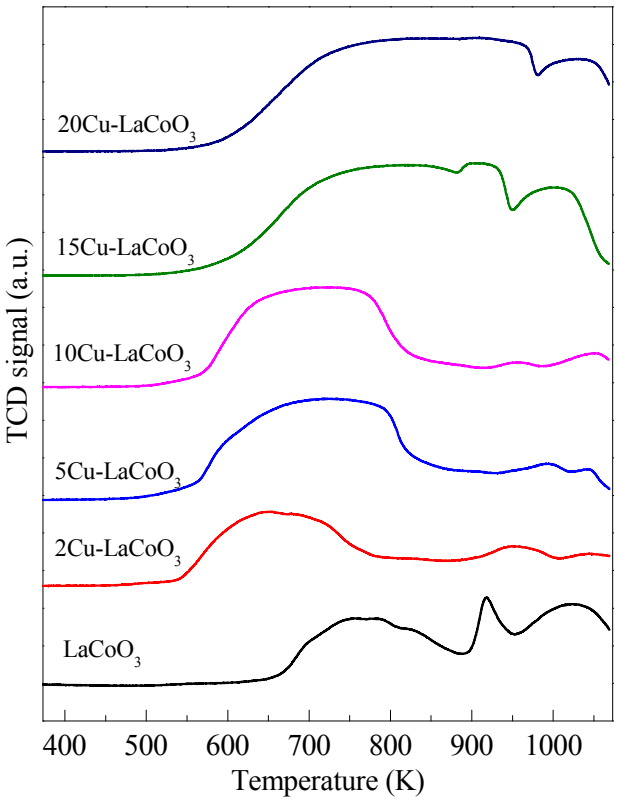

Fig. 5. H_2-TPR profiles of calcined xCuO-$LaCoO_3$ catalysts.

duction peak towards lower temperature regions was observed upon the incorporation of 2 wt% Cu. The onset reduction temperature decreased noticeably from 644 K ($LaCoO_3$ support) to 527 K (2CuO-$LaCoO_3$) and the peak temperature also decreased to 653 K for the latter sample. The major peak in the low-temperature region for the catalysts with (5 and 10) wt% Cu broadened and the peak shifted to around 713 K. Further increase in Cu loading to 15% and above led to an obvious broadening and shifting of the reduction peak towards higher temperatures. Because CuO can be reduced at lower temperatures when compared to CoO_x, the obvious shift in the reduction temperature for low-Cu loading ((2–10) wt%) catalysts might be ascribed to the spillover of the adsorbed hydrogen from Cu^0 to cobalt oxides [10,46]. Thus, it is likely that the collective reduction of Cu^{2+} to Cu^0 and Co^{3+} to Co^{2+} as well as a small amount of Co^{2+} to Co^0 contributes to the major peak at temperatures below 890 K for samples with Cu loading below 10 wt%. The shifting of the reduction temperature to higher regions for samples with high Cu loadings (>10%) could be attributed to the formation of CuO and perovskite-type $LaCoO_3$ with large crystallite sizes, as inferred from the XRD characterization results (Fig. 1).

Because the surface basicity of catalysts plays an important role in the catalytic hydrogenolysis of FA and FFA [8,13,14], the basicity of xCu-$LaCoO_3$ catalysts was characterized by CO_2-TPD (Fig. 6). A very small peak at around 598 K was detected in each sample, which could be attributed to moderate basic sites. It can also be seen that all the samples showed obvious CO_2 desorption at temperatures above 850 K, which may be associated with the formation of carbonate species when the sample was exposed to CO_2 [37]. Such carbonate species would contribute to the strong basicity of the catalysts. Thus, the 10Cu-$LaCoO_3$ catalyst with the largest CO_2 desorption peak area at temperatures above 850 K would possess the largest amount of strong basic sites. Characterization of the acidity of 10Cu-$LaCoO_3$ catalyst by NH_3-TPD (Fig. S1 in Supporting Information) indicated a rather low acidity for this catalyst.

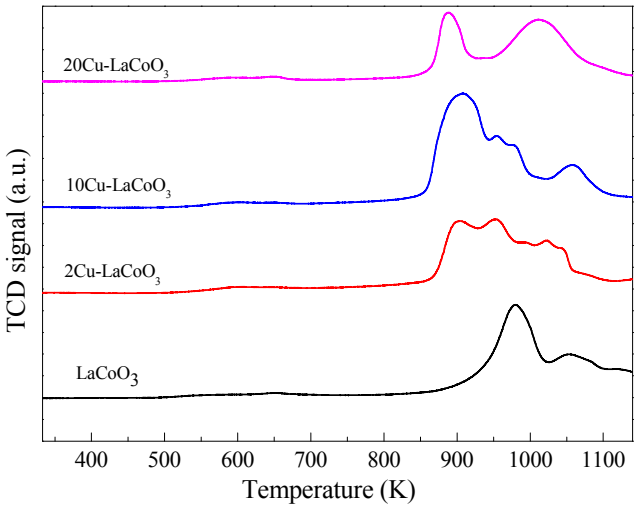

Fig. 6. CO_2-TPD profiles of calcined xCuO-$LaCoO_3$ catalysts.

Table 1 shows the textural properties of the calcined samples. The BET surface areas of the calcined CuO-$LaCoO_3$ samples increased from 3.5 m^2/g to a maximum of 21.7 m^2/g as the Cu loading increased from 0 to 5 wt% and then decreased to 1.7 and 3.8 m^2/g at Cu loadings of 15 wt% and 20 wt%, respectively. The pore volumes of the samples were below 0.06 cm^3/g. Such low surface areas and pore volumes of the samples could be ascribed to the perovskite-type structure and high calcination temperatures [47,48]. The rather high BET surface area of 5CuO-$LaCoO_3$ may be associated with the negligible formation of a perovskite structure in this sample, as revealed by XRD characterization (Fig. 1). The average pore diameters of the CuO-$LaCoO_3$ samples were in the mesopore range of 10–25 nm. The Cu and Co loadings of the samples, as measured by XRF, were close to their actual amounts (Table 1). Comparing the characterization results of BET and CO_2-TPD, it could be inferred that the catalytic performance of the catalyst is more profoundly affected by the reduction properties of the catalyst rather than the BET surface area and basicity.

Table 1
The textural properties of calcined xCuO-$LaCoO_3$ samples.

Sample	BET area (m^2/g)	Pore volume (cm^3/g)	Average pore diameter (nm)	Cu (wt%)	Co (wt%)
$LaCoO_3$	3.5	0.02	24.0	0.0	18.8
2CuO-$LaCoO_3$	6.6	0.02	13.8	1.8	18.2
5CuO-$LaCoO_3$	21.7	0.06	10.2	5.0	17.4
10CuO-$LaCoO_3$	5.8	0.03	18.3	10.2	17.5
15CuO-$LaCoO_3$	1.7	0.004	10.0	14.7	15.9
20CuO-$LaCoO_3$	3.8	0.02	24.8	20.5	15.9

Table 2
Conversion and selectivity corresponding to FFA hydrogenolysis over different catalysts. [a]

Entry	Catalyst	Conversion (%)	Selectivity (%)			
			1,2-PeD	1,5-PeD	THFA	Others [b]
1	LaCoO3 [c]	2.2	0.0	0.0	34.6	65.4
2	2Cu-$LaCoO_3$	56.2	14.3	35.0	32.1	18.6
3	5Cu-$LaCoO_3$	88.4	14.1	38.1	34.1	13.7
4	10Cu-$LaCoO_3$	94.6	13.9	36.9	33.7	15.5
5	15Cu-$LaCoO_3$	53.8	12.7	29.3	35.5	22.5
6	20Cu-$LaCoO_3$	51.6	12.8	28.8	36.5	21.9
7	10Cu-$LaCoO_3$ [d]	100.0	15.2	40.3	28.7	15.8
8	5Pt-$LaCoO_3$	74.0	9.3	26.8	44.5	19.4
9	5Ru-$LaCoO_3$	93.5	12.1	6.4	72.9	8.6
10	5Pd-$LaCoO_3$	80.7	trace	trace	>99	0.0
11	5Rh-$LaCoO_3$	100.0	1.2	3.4	94.0	1.4
12	$CuCr_2O_4$	9.5	27.3	14.2	11.1	47.4
13	10Cu+LaCoO3 [e]	7.8	3.3	6.2	15.1	75.4
14	Pure Cu	4.4	2.7	0.0	9.9	83.4

[a] Reaction conditions: 0.11 g Cu, 30 g of 5 wt% FFA in ethanol, 413 K, 6 MPa H_2, 2 h; [b] Others include n-pentane, 1,4-PeD, 2-methyl furan, 2-methyl tetrahydrofuran, n/2-pentanol, and some undetermined products; [c] 1.1 g $LaCoO_3$; [d] 0.15 g Cu; [e] Physical mixture of pure Cu and $LaCoO_3$.

3.2. FFA hydrogenolysis over different catalysts

Table 2 shows the conversions and selectivities of FFA hydrogenolysis over different catalysts at 413 K and 6 MPa H_2. The conversion of FFA for *x*Cu-$LaCoO_3$ catalysts increased sharply from 56.2% (2Cu-$LaCoO_3$) to 94.6% (10Cu-$LaCoO_3$) and then decreased gradually to 51.6% with a further increase in the Cu content to 20 wt% (entries 2–6). The selectivities for 1,5-PeD were in the range of 35.0%–38.1% for *x*Cu-$LaCoO_3$ catalysts with low Cu loadings ((2–10) wt%), which further decreased to ~29.0% for high Cu-loading ((15–20) wt%) catalysts. Meanwhile, 1,2-PeD selectivities dropped from ~14.0% at low Cu loadings ((2–10) wt%) to ~12.7% at high Cu loadings ((15–20) wt%). For the *x*Cu-$LaCoO_3$ catalysts, THFA was determined to be the major byproduct with a selectivity in the range of 32.1%–36.5%. When the amount of the catalyst is increased (0.15 g Cu^0), the yield of 1,5-PeD (40.3%) is close to that obtained with recently reported Cu-Co-Al (44% yield of 1,5-PeD) [10] and Ni-Y_2O_3 (41.9% yield of 1,5-PeD) [11] catalysts.

For comparison, the catalytic performances of $LaCoO_3$-supported noble metals, Pt, Ru, Pd, and Rh, with 5 wt% loading prepared by the same citrate-complexing method and a commercial $CuCr_2O_4$ catalyst were also studied (entries 8–12). 5Pt-$LaCoO_3$ exhibited moderate but inferior FFA conversion and PeD selectivity compared to 5Cu-$LaCoO_3$ and 10Cu-$LaCoO_3$. The higher selectivity for 1,5-PeD (26.8%) obtained over 5Pt-$LaCoO_3$ as compared to 1,2-PeD (9.3%) is in line with a previous study on the hydrogenolysis of FFA over Pt-Co_2AlO_4 [15]. Although high FFA conversions (>80%) were attained over $LaCoO_3$-supported Ru, Rh, and Pd catalysts, these catalysts showed a quite low selectivity towards PeDs (combined selectivity <20%) with THFA as the predominant product (selectivity >70%) (entries 9–11). The commercial $CuCr_2O_4$ catalyst exhibited a rather low FFA conversion (9.5%) and a higher 1,2-PeD selectivity (27.3%) over 1,5-PeD (14.2%) under similar reaction conditions (entry 12). Clearly, among the catalysts investigated, 10Cu-$LaCoO_3$ exhibited the best performance for the production of PeDs by FFA hydrogenolysis with both high FFA conversion and PeD selectivity. Thus, this catalyst was selected for further studies.

To investigate the role of Cu^0 and $LaCoO_3$ in FFA hydrogenolysis, $LaCoO_3$, Cu^0 + $LaCoO_3$ physical mixture, and Cu^0 catalysts were also tested (entry 1, 13, and 14). The $LaCoO_3$ support showed an extremely low FFA conversion (2.2%) and almost no activity for the cleavage of the furan ring C–O bonds and resulted in THFA as the main product (entry 1). Pure Cu^0 exhibited a low 1,2-PeD selectivity (2.7%) at a slightly higher FFA conversion (4.4%) as compared to the $LaCoO_3$ support (entry 14). Interestingly, the Cu^0 + $LaCoO_3$ physical mixture catalyst exhibited not only a higher FFA conversion (7.8%), but also a higher selectivity towards PeDs with 1,5-PeD being the major product (entry 13). These findings indicate that Cu^0 provides the majority of the active sites for the generation of 1,2-PeD from FFA, while the coexistence of Cu^0 and $LaCoO_3$ with strong basicity (Fig. 6) could steer the cleavage of the furan ring C–O bond to produce 1,5-PeD. The remarkably high FFA conversion and PeD selectivity obtained with 10Cu-$LaCoO_3$ (entry 4) indicates the importance of cooperation between Cu and $LaCoO_3$ with high dispersion for the efficient hydrogenolysis of FFA into PeDs. It seems that the partially reduced Cu^0-CoO boundary played an important role in the selective hydrogenolysis of FFA to 1,5-PeD [10], while Cu^0 was mainly responsible for the production of 1,2-PeD.

3.3. Effects of reaction parameters on FFA hydrogenolysis to 1,2-PeD and 1,5-PeD

Fig. 7 displays the effect of reaction temperature on FFA hydrogenolysis activity over 10Cu-$LaCoO_3$ at 6 MPa H_2 in the FFA conversion range of 15%–25%. The reaction rate of PeDs, defined as moles of PeDs produced by a mole of the active metal (Co+Cu) with respect to time, increased drastically from 0.1 h^{-1} at 393 K to 5.4 h^{-1} at 453 K (Fig. 7(a)), with an activation energy of 47.8 kJ/mol. The selectivity for 1,2-PeD and 1,5-PeD firstly increased from 8.8% and 21.0% at 393 K to the maximum values of 13.7% and 38.5% at 433 K, respectively, and then were almost constant as the temperature increased to 453 K. An increase in the temperature resulted in a sharp drop in THFA selectivity from 61.1% at 393 K to 19.8% at 453 K, which shows that the increase of the relative reaction rate for C=C bond hydrogenation is lower than that of C–O bond hydrogenolysis with the increase of temperature. The selectivity for n-pentanol and 2-pentanol (referred to as pentanols), which are dehydration products of PeDs, increased linearly from 1.1% at 393 K to 9.5% at 453 K. Similarly, the selectivity for the C–OH dehydration products of FFA, 2-methylfuran (2-MF) and 2-methyltetrahydrofuran (2-MTHF), increased uniformly from 1.2% at 393 K to 14.9% at 453 K.

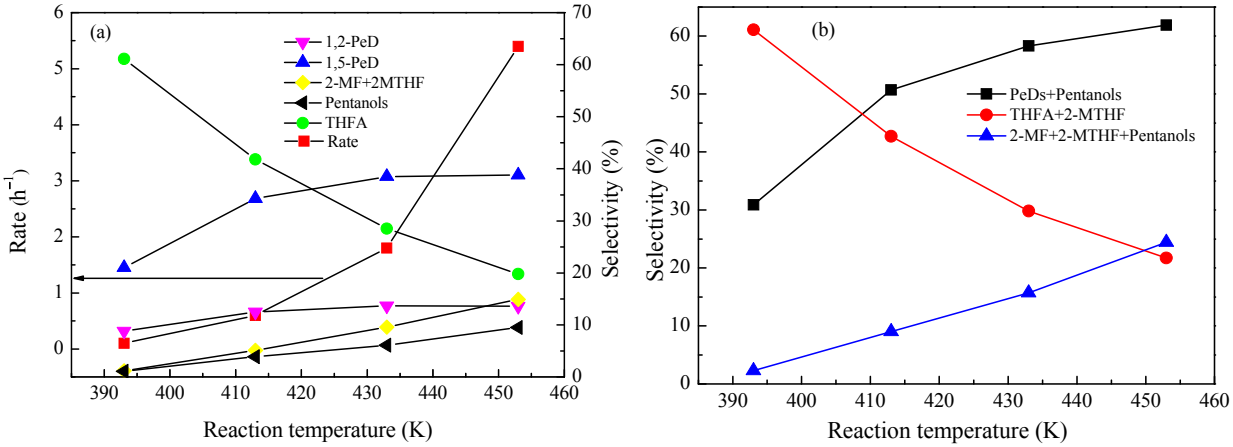

Fig. 7. Effect of reaction temperature on FFA hydrogenolysis over 10Cu-$LaCoO_3$. Reaction conditions: 0.003–0.129 g Cu, 30 g of 5 wt% FFA in ethanol, 6 MPa H_2, 1 h.

Because the hydrogenolysis of cyclic ether C–O bonds produces PeDs, C–OH bond dehydration and furan ring C=C bond hydrogenation of FFA are competitive reactions; at the same time, further hydrogenolysis of PeDs to pentanols (dehydration) and hydrogenation of 2-MF (furan ring C=C bonds) to 2-MTHF are secondary reactions involved in FFA hydrogenolysis [6,27]. Fig 7(b) depicts a clearer picture seeing the changes of the activity of cyclic ether C–O bonds hydrogenolysis, C–OH bond dehydration and furan ring C=C bonds hydrogenation of the catalyst with the change of reaction temperature. The selectivity for PeDs and pentanols (cyclic ether C–O bond hydrogenolysis products) increased monotonously with increasing temperature; meanwhile, the selectivity for 2-MF, 2-MTHF, and pentanols (C–OH dehydration products) also increased linearly, suggesting that higher temperatures favor not only the cleavage of cyclic ether C–O bonds, but also the hydrogenolysis of C–OH bonds. In contrast, the selectivity for furan ring C=C bond hydrogenation products, THFA and 2-MTHF, decreased sharply from 61.1% at 393 K to 21.7% at 453 K with increasing temperature. Clearly, higher temperatures are more favorable for the hydrogenolysis of C–O over 10Cu-$LaCoO_3$ than for the hydrogenation of furan ring C=C bonds. Thus, an appropriately high temperature (433 K) is found to benefit the hydrogenolysis of FFA to PeDs.

Fig. 8 shows the effect of H_2 pressure on FFA hydrogenolysis over 10Cu-$LaCoO_3$ at a controlled FFA conversion of 15%–25%. The reaction rate for PeD production rapidly increased from 0.1 h^{-1} at 2 MPa to 1.7 h^{-1} at 8 MPa (Fig. 8(a)). The selectivity of 1,5-PeD firstly increased from 25.2% at 2 MPa to a maximum of 34.3% at 6 MPa and then remained almost constant as the H_2 pressure increased to 8 MPa; 1,2-PeD selectivity remained stable at 12% with an increase in H_2 pressure (Fig. 8(a)). The selectivity of THFA increased steadily from 27.3% at 2 MPa to 44.1% at 8 MPa with increasing H_2 pressure. Simultaneously, the combined selectivity of 2-MF and 2-MTHF decreased from 14.6% to 3.7% during the same process. In addition, a slight decrease in pentanol selectivity from 5.5% to 3.5% was observed with an increase in pressure. The above findings suggest that a high H_2 pressure favors not only the hydrogenolysis of cyclic ether C–O bonds but also the hydrogenation of furan ring C=C bonds; the reaction rate of the latter increased more rapidly, leading to a slight decrease in the products of the former reaction at relatively high pressures of 8 MPa. The gradual decline of the combined selectivity of the C–OH bond dehydration products of pentanols, 2-MF, and 2-MTHF indicates that the C–OH bond dehydration reaction was suppressed with in-

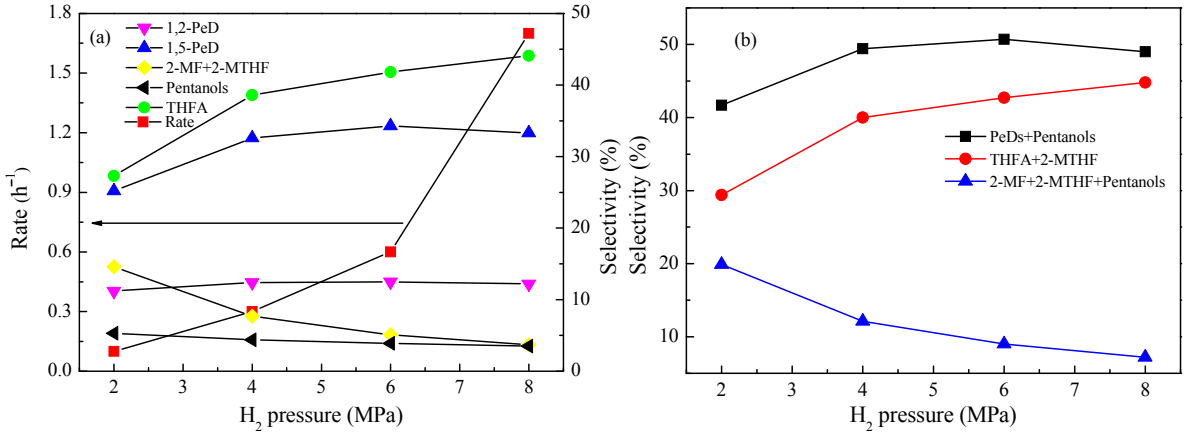

Fig. 8. Effect of H_2 pressure on FFA hydrogenolysis reactivity over the 10Cu-$LaCoO_3$ catalyst. Reaction conditions: 0.018–0.166 g Cu, 30 g of 5 wt% FFA in ethanol, 413 K, 1 h.

creasing H_2 pressure (Fig. 8(b)). Clearly, an appropriately high H_2 pressure (~6 MPa) favors the production of the target PeDs at high yields.

The conversions and selectivities of 10Cu-$LaCoO_3$ during FFA hydrogenolysis as functions of reaction time at 413 K and 6 MPa H_2 are shown in Fig. 9. The conversion of FFA increased drastically from 25.3% at 0.2 h to 94.6% at 2 h and full conversion was achieved after 4 h. The selectivity of 1,5-PeD increased from 25.9% at 0.2 h to a maximum of 40.6% at 4 h and then remained almost constant as the reaction time increased to 8 h. The selectivity of 1,2-PeD increased slightly from 11.0% at 0.2 h to 14.8% after 8 h. Simultaneously, a slight decrease in the selectivity of THFA from around 36.0% at 0.2 h to 28.4% was observed with an increase in the reaction time to 8 h; this might be a result of the more favored reaction of FFA hydrogenolysis to PeDs, which were not further hydrogenolyzed to pentanols or 2-MTHF. A separate reaction on the direct hydrogenolysis of THFA under the same conditions as those employed for FFA hydrogenolysis resulted in no reaction products, supporting that both PeDs and 2-MTHF are generated from FFA but not THFA, which is in line with previous findings [8,15,27]. Although 2-MF could be further hydrogenated to 2-MTHF and pentanols [15,27], the slight increase in pentanol selectivity (from 3.5% to 5.6%) and simultaneous decline in the combined selectivity of 2-MF and 2-MTHF (from 6.0% to 3.5%) after 8 h of reaction indicates that further hydrogenation of 2-MF to pentanols is not the main cause for the observed decrease in the combined selectivity of 2-MF and 2-MTHF. The more favored reaction of FFA hydrogenolysis to PeDs as compared to FFA hydrogenolysis to 2-MF probably accounts for the decline in the combined selectivity of 2-MF and 2-MTHF. Thus, it is likely that further hydrogenolysis of PeDs contributed to the increase in pentanol selectivity.

3.4. Recycling of the 10Cu-$LaCoO_3$ catalyst used for FFA hydrogenolysis

The 10Cu-$LaCoO_3$ catalyst was repeatedly used for FFA hydrogenolysis to study its reusability (Fig. 10). The conversion of FFA increased from 93.7% to 99.3% after one cycle and then was almost constant for three more cycles. Nonetheless, a continual decrease was observed in the selectivity of 1,5-PeD (from 37.9% to 28.7%) and 1,2-PeD (from 13.0% to 7.8%) during four cycle reactions. In the meantime, the selectivity of THFA increased slightly from 31.7% to 41.8%. The increase in THFA selectivity at the expense of PeD selectivity suggests that the hydrogenation activity of furan ring C=C bonds increased, while the hydrogenolysis activity of cyclic ether C–O bonds declined. Thus, the increase in FFA conversion after recycling can be mainly attributed to the enhanced hydrogenation activity of furan ring C=C bonds, leading to the generation of high amounts of THFA, which cannot be further converted to PeDs under the used reaction conditions. Similar trends for FFA conversion and product selectivities were observed when the recycling of the catalyst was studied at low initial FFA conversion (30.5%, see Fig. S2 in SI).

In order to evaluate the reasons for these changes in the performance of the catalyst, it was characterized by XRD (Fig. 2) and TEM (Fig. 4) at three different states. The appearance of a Cu^0 diffraction peak along with a largely disappeared Co_3O_4 diffraction peak after catalyst reduction (in 5%H_2-95%N_2) and usage for one time (Fig. 2((3) and (4))) gives us to understand that the active sites for FFA hydrogenolysis are probably associated with the presence of Cu^0 and Co with low valencies. Because Cu^0 itself (Table 2, entry 14) and its combination with acidic and basic supports favor the generation of 1,2-PeD over 1,5-PeD during FFA hydrogenolysis [8,27,29], the higher 1,5-PeD selectivity obtained over Cu-$LaCoO_3$ catalysts as well as the physical mixture of Cu^0 + $LaCoO_3$ indicates that Co species played an important role in the selective cleavage of the secondary C–O bond of FFA. The presence of Co species preferably cleaved secondary C–O bonds but not the primary C–O bond of FFA, which is in line with previous findings [10,15,30]. It was reported that the presence of large amounts of Co^{2+} facilitates the adsorption of FFA in a tilted conformation, which enhances the cleavage of the secondary C–O bonds of FFA [10], leading to a high selectivity toward 1,5-PeD. Because CoO is much harder to be reduced than Co_3O_4 [10,46], the partial reduction of Co_3O_4

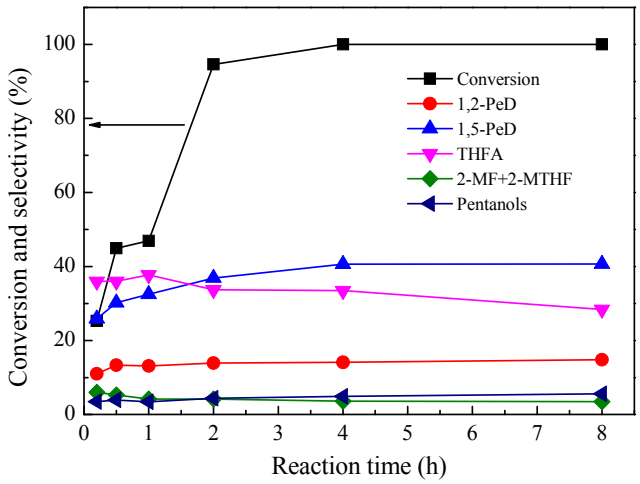

Fig. 9. Effect of reaction time on FFA hydrogenolysis over 10Cu-$LaCoO_3$. Reaction conditions: 0.11 g Cu, 30 g of 5 wt% FFA in ethanol, 413 K, 6 MPa H_2.

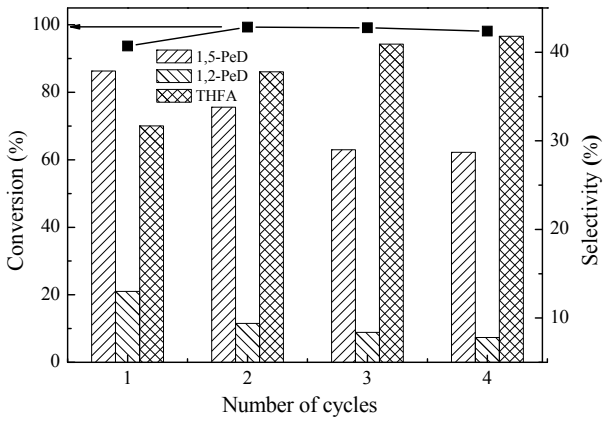

Fig. 10. Reusability of the 10Cu-$LaCoO_3$ catalyst for FFA hydrogenolysis Reaction conditions: 0.11 g Cu, 30 g of 5 wt% FFA in ethanol, 413 K, 6 MPa H_2, 2 h.

to highly dispersed CoO in a hydrogenation atmosphere as well as the presence of an alcoholic solvent might be responsible for the largely diminished Co_3O_4 diffraction peak after the 10Cu-$LaCoO_3$ catalyst was used one time (Fig. 2(4)). Further diminishing of the Co_3O_4 diffraction peak after the catalyst was repeatedly used for three more cycles indicates the sequential reduction of Co_3O_4 to CoO and later to Co^0 (Fig. 2(5)). The decrease in PeD selectivity, especially 1,5-PeD selectivity, with the continuous use of the catalyst implies a decrease in the CoO amount in the catalyst. Thus, an increase in FFA conversion and THFA selectivity may be associated with an increase in the amount of Co^0. Note that the sintering of Cu particles, as revealed by XRD (Fig. 2((3) and (4))) and TEM (Fig. 4((d) and (f))), in the used catalyst would also cause a decline in the hydrogenolysis activity of cyclic ether C–O bonds [27]. The significant weakening of all the diffraction peaks of the 10Cu-$LaCoO_3$ catalyst after four cycles can be associated with carbon deposition, as evidenced by the obvious mass loss (7.2%) in between 550–855 K in the TG profile of the used 10Cu-$LaCoO_3$ catalyst (Fig. 11(2)) [49]. The mass loss at temperatures above 855 K for both the freshly reduced catalyst and used catalyst can be associated with the decomposition of $La_2O_2CO_3$ [33].

3.5. *Effect of pretreatment atmosphere on the catalytic performance of 10Cu-$LaCoO_3$*

In order to further elucidate the active species in the Cu-$LaCoO_3$ catalyst used for FFA hydrogenolysis, the effect of reduction atmosphere on the structure and reaction properties of the 10Cu-$LaCoO_3$ catalyst was investigated. Prereduction of the catalyst with low concentrations of H_2 (e.g., 5%) led to high selectivity (>36%) towards 1,5-PeD but slightly lower FFA conversions (Table 3). The selectivity of THFA increased and it became the major product at the expense of 1,5-PeD with increasing H_2 concentration; full conversion of FFA was obtained upon prereduction of the catalyst with pure H_2. From the H_2-TPR results (Fig. 5), it can be understood that it is hard to reduce the calcined CuO-$LaCoO_3$ catalyst at a low prereduction temperature of 573 K with 5% H_2; this is proved by the XRD

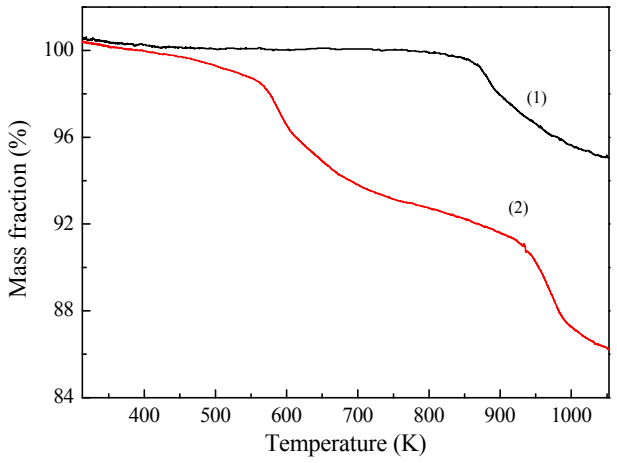

Fig. 11. TG patterns of 10Cu-$LaCoO_3$ catalysts at different states. (1) Reduced in 5%H_2-95%N_2; (2) Reduced in 5%H_2-95%N_2 and used four times.

Table 3
Effect of pretreatment atmosphere on the conversion of furfuryl alcohol over the 10Cu-$LaCoO_3$ catalyst. [a]

Pretreatment atmosphere	Conversion (%)	Selectivity (%)			
		1,2-PeD	1,5-PeD	THFA	Others [b]
Pure H_2	100.0	14.5	28.6	48.9	8.0
50%H_2-50%N_2	94.3	14.4	30.5	44.0	11.1
5%H_2-95%N_2	94.6	13.9	36.9	33.7	15.5
5%H_2-95%Ar	92.2	15.4	37.4	27.8	19.4

[a] Reaction conditions: 0.11 g Cu, 30 g of 5 wt% FFA in ethanol, 413 K, 6 MPa H_2, 2 h
[b] Including n-pentane, 1,4-PeD, 2-MF, 2-MTHF, n/2-pentanol, and some undetermined products

characterization results (Fig. 2(3)). Prereduction of the catalyst with high concentrations of H_2 (i.e., 100%) enhanced the reducibility of the catalyst as revealed by the presence of the diffraction peak of Cu^0 and simultaneous disappearance of the diffraction peak of Co_3O_4 (Fig. 2(2)). Although no diffraction peaks of Co^0 and/or CoO were observed after the catalyst was reduced in pure H_2, Co^0 and/or highly dispersed CoO were deduced to be present in the catalyst. It has been reported that Co^0 exhibited a higher C=C hydrogenation reactivity than Cu^0 [50]. Thus, a high amount of Co^0 would promote the hydrogenation of C=C in the furan ring, leading to the generation of a large amount of a furan-ring saturated product (THFA); this observation was reported in previous studies as well [10,27]. Clearly, the increase in FFA conversion and THFA selectivity with an increase in the concentration of H_2 in the prereduction gas (Table 3) is associated with the increase of Co^0 in the catalyst. The decline in 1,5-PeD selectivity with increasing H_2 gas concentration can be related to the decreasing amount of partially reduced CoO species, due to their further reduction at high H_2 concentrations. Therefore, studying the effect of the prereduction atmosphere supported the previously mentioned findings on the recycling of 10Cu-$LaCoO_3$; cooperative catalysis occurred between Cu^0 and CoO, which promoted the hydrogenolysis of FFA to PeDs, especially to 1,5-PeD, while Co^0 promoted the hydrogenation of FFA to THFA. Taking the catalytic performances of Cu-$LaCoO_3$ catalysts into consideration (Table 2), it is suggested that the synergetic effect between balanced Cu^0 and CoO sites plays a critical role in achieving a high yield of 1,5-PeD from FFA hydrogenolysis.

4. Conclusions

In summary, Cu-$LaCoO_3$ with a perovskite structure was employed as an effective catalyst for the selective hydrogenolysis of biomass-derived FFA to 1,5-PeD and 1,2-PeD. The catalytic performances of the catalysts were found to depend on Cu loading and prereduction conditions, such as the H_2 concentration of the reducing gas. The reaction parameters, including temperature and H_2 pressure, also greatly affected the reaction activity and product selectivity. It was demonstrated that cooperation between partially reduced Co_3O_4 (probably as CoO) and fully reduced Cu species (Cu^0) induces a synergetic effect for the selective adsorption and catalyzed opening of the furan

ring, leading to 1,5-PeD with a high yield. Increasing the reducibility of the catalyst to enhance the reduction of Co species to Co^0 would promote the production of THFA. By optimizing the catalyst composition and prereduction and reaction conditions, a high FFA conversion of ~100% and selectivity of 55.5% for 1,5-PeD (40.3%) and 1,2-PeD (15.2%) were achieved at 413 K and 6 MPa H_2 over a catalyst containing 10 wt% Cu loading and prereduced in 5% H_2. The important findings of this work would shed light on the development of efficient non-noble metal catalysts for the production of valuable PeDs from biomass.

References

[1] L. T. Mika, E. Csefalvay, A. Nemeth, *Chem Rev.,* **2018**, 118, 505–613.
[2] C. Z. Li, X. C. Zhao, A. Q. Wang, G. W. Huber, T. Zhang, *Chem Rev.,* **2015**, 115, 11559–11624.
[3] R. Mariscal, P. Maireles-Torres, M. Ojeda, I. Sádaba, M. López Granados, *Energy Environ. Sci.,* **2016**, 9, 1144–1189.
[4] M. Besson, P. Gallezot, C. Pinel, *Chem Rev.,* **2014**, 114, 1827–1870.
[5] M. J. Climent, A. Corma, S. Iborra, *Green Chem.,* **2014**, 16, 516–547.
[6] Y. Nakagawa, M. Tamura, K. Tomishige, *ACS Catal.,* **2013**, 3, 2655–2668.
[7] J. Y. He, K. F. Huang, K. J. Barnett, S. H. Krishna, D. M. Alonso, Z. J. Brentzel, S. P. Burt, T. Walker, W. F. Banholzer, C. T. Maravelias, I. Hermans, J. A. Dumesic, G. W. Huber, *Faraday Discuss.,* **2017**, 202, 247–267.
[8] H. L. Liu, Z. W. Huang, F. Zhao, F. Cui, X. M. Li, C. G. Xia, J. Chen, *Catal. Sci. Technol.,* **2016**, 6, 668–671.
[9] Z. J. Brentzel, K. J. Barnett, K. F. Huang, C. T. Maravelias, J. A. Dumesic, G. W. Huber, *ChemSusChem,* **2017**, 10, 1351–1355.
[10] T. P. Sulmonetti, B. Hu, S. Lee, P. K. Agrawal, C. W. Jones, *ACS Sustainable Chem. Eng.,* **2017**, 5, 8959–8969.
[11] H. W. Wijaya, T. Kojima, T. Hara, N. Ichikuni, S. Shimazu, *ChemCatChem,* **2017**, 9, 2869–2874.
[12] R. F. Ma, X. P. Wu, T. Tong, Z. J. Shao, Y. Q. Wang, X. H. Liu, Q. N. Xia, X. Q. Gong, *ACS Catal.,* **2017**, 7, 333–337.
[13] B. Zhang, Y. L. Zhu, G. Q. Ding, H. Y. Zheng, Y. W. Li, *Green Chem.,* **2012**, 14, 3402–3409.
[14] T. Mizugaki, T. Yamakawa, Y. Nagatsu, Z. Maeno, T. Mitsudome, K. Jitsukawa, K. Kaneda, *ACS Sustainable Chem. Eng.,* **2014**, 2, 2243–2247.
[15] W. J. Xu, H. F. Wang, X. H. Liu, J. W. Ren, Y. Q. Wang, G. Z. Lu, *Chem. Commun.,* **2011**, 47, 3924–3926.
[16] M. Chia, Y. J. Pagan-Torres, D. Hibbitts, Q. H. Tan, H. N. Pham, A. K. Datye, M. Neurock, R. J. Davis, J. A. Dumesic, *J. Am. Chem. Soc.,* **2011**, 133, 12675–12689.
[17] M. Chatterjee, H. Kawanami, T. Ishizaka, M. Sato, T. Suzuki, A. Suzuki, *Catal. Sci. Technol.,* **2011**, 1, 1466–1471.
[18] J. Guan, G. M. Peng, Q. Cao, X. D. Mu, *J. Phys. Chem. C,* **2014**, 118, 25555–25566.
[19] S. Koso, N. Ueda, Y. Shinmi, K. Okumura, T. Kizuka, K. Tomishige, *J. Catal.,* **2009**, 267, 89–92.
[20] K. Y. Chen, S. Koso, T. Kubota, Y. Nakagawa, K. Tomishige, *ChemCatChem,* **2010**, 2, 547–555.
[21] S. Koso, I. Furikado, A. Shimao, T. Miyazawa, K. Kunimori, K. Tomishige, *Chem. Commun.,* **2009**, 2035–2037.
[22] K. Y. Chen, K. Mori, H. Watanabe, Y. Nakagawa, K. Tomishige, *J. Catal.,* **2012**, 294, 171–183.
[23] S. B. Liu, Y. Amada, M. Tamura, Y. Nakagawa, K. Tomishige, *Green Chem.,* **2014**, 16, 617–626.
[24] S. B. Liu, Y. Amada, M. Tamura, Y. Nakagawa, K. Tomishige, *Catal. Sci. Technol.,* **2014**, 4, 2535–2549.
[25] Y. Nakagawa, M. Tamura, K. Tomishige, *Catal. Surv. Asia,* **2015**, 19, 249–256.
[26] K. Tomishige, Y. Nakagawa, M. Tamura, *Green Chem.,* **2017**, 19, 2876–2924.
[27] H. L. Liu, Z. W. Huang, H. X. Kang, C. G. Xia, J. Chen, *Chin. J. Catal.,*

Graphical Abstract

Chin. J. Catal., 2018, 39: 1711–1723 doi: 10.1016/S1872-2067(18)63110-9

Selective hydrogenolysis of furfuryl alcohol to 1,5- and 1,2-pentanediol over Cu-$LaCoO_3$ catalysts with balanced Cu^0-CoO sites

Fangfang Gao, Hailong Liu, Xun Hu, Jing Chen *, Zhiwei Huang *, Chungu Xia
Lanzhou Institute of Chemical Physics (LICP), Chinese Academy of Sciences; University of Chinese Academy of Sciences

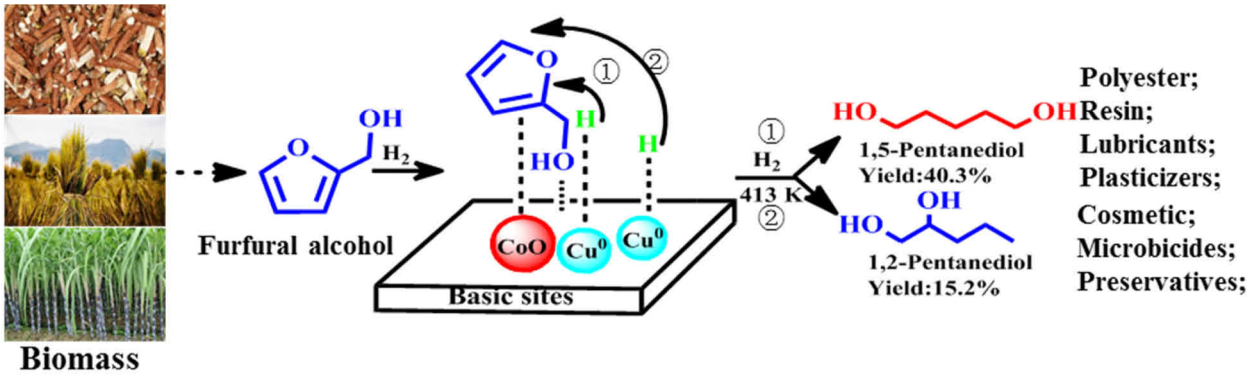

The synergism between balanced Cu^0 and CoO sites played a critical role in achieving a high yield of PeDs with high 1,5-/1,2-pentanediol selectivity ratio during the hydrogenolysis of biomass-derived furfuryl alcohol.

2016, 37, 700–710.
[28] D. Götz, M. Lucas, P. Claus, *Catalysts,* **2017**, 7, 50/1–50/7.
[29] H. Adkins, R. Connor, *J. Am. Chem. Soc.,* **1931**, 53, 1091–1095.
[30] J. Lee, S. P. Burt, C. A. Carrero, A. C. Alba-Rubio, I. Ro, B. J. O'Neill, H. J. Kim, D. H. K. Jackson, T. F. Kuech, I. Hermans, J. A. Dumesic, G. W. Huber, *J. Catal.,* **2015**, 330, 19–27.
[31] J. C. Lee, Y. Xu, G. W. Huber, *Appl. Catal. B,* **2013**, 140–141, 98–107.
[32] M. Y. Chen, C. B. Chen, B. Zada, Y. Fu, *Green Chem.,* **2016**, 18, 3858–3866.
[33] B. H. Zhao, B. H. Yan, S. Y. Yao, Z. H. Xie, Q. Y. Wu, R. Ran, D. Weng, C. Zhang, J. G. Chen, *J. Catal.,* **2018**, 358, 168–178.
[34] X. L. Zhang, Y. D. Gong, S. Q. Li, C. W. Sun, *ACS Catal.,* **2017**, 7, 7737–7747.
[35] J. Hwang, R. R. Rao, L. Giordano, Y. Katayama, Y. Yu, Y. Shao-Horn, *Science,* **2017**, 358, 751–756.
[36] F. Polo-Garzon, Z. L. Wu, *J. Mater. Chem. A,* **2018**, 6, 2877–2894.
[37] S. Dama, S. R. Ghodke, R. Bobade, H. R. Gurav, S. Chilukuri, *Appl. Catal. B,* **2018**, 224, 146–158.
[38] H. L. Liu, Z. W. Huang, Z. B. Han, K. L. Ding, H. C. Liu, C. G. Xia, J. Chen, *Green Chem.,* **2015**, 17, 4281–4290.
[39] H. L. Liu, Z. W. Huang, H. X. Kang, X. M. Li, C. G. Xia, J. Chen, H. C. Liu, *Appl. Catal. B,* **2018**, 220, 251–263.
[40] F. Ma, W. Chu, L. H. Huang, X. P. Yu, Y. Y. Wu, *Chin. J. Catal.,* **2011**, 32, 970–977.
[41] X. H. Guo, Y. Li, W. Song, W. J. Shen, *Catal. Lett.,* **2011**, 141, 1458–1463.
[42] X. W. Du, S. P. Luo, H. Y. Du, M. Tang, X. D. Huang, P. K. Shen, *J. Mater. Chem. A,* **2016**, 4, 1579–1585.
[43] Y. C. Wei, X. Ren, H. M. Ma, X. Sun, Y. Zhang, X. Kuang, T. Yan, H. X. Ju, D. Wu, Q. Wei, *Chem. Commun*., **2018**, 54, 1533–1536.
[44] L. Predoana, B. Malic, M. Kosec, M. Carata, M. Caldararu, M. Zaharescu, *J. Eur. Ceram. Soc.,* **2007**, 27, 4407–4411.
[45] L. Zhao, T. Han, H. Wang, L. H. Zhang, Y. Liu, *Appl. Catal. B,* **2016**, 187, 19–29.
[46] Z. W. Huang, K. J. Barnett, J. P. Chada, Z. J. Brentzel, Z. R. Xu, J. A. Dumesic, G. W. Huber, *ACS Catal.,* **2017**, 7, 8429–8440.
[47] A. A. A. da Silva, M. C. Ribeiro, D. C. Cronauer, A. J. Kropf, C. L. Marshall, P. Gao, G. Jacobs, B. H. Davis, F. B. Noronha, L. V. Mattos, *Top. Catal.,* **2014**, 57, 637–655.
[48] C. Zhou, X. Liu, C. Z. Wu, Y. W. Wen, Y. J. Xue, R. Chen, Z. L. Zhang, B. Shan, H. F. Yin, W. G. Wang, *Phys. Chem. Chem. Phys.,* **2014**, 16, 5106–5112.
[49] D. P. Liu, X. Y. Quek, H. H. A. Wah, G. M. Zeng, Y. H. Li, Y. Yang, *Catal. Today,* **2009**, 148, 243–250.
[50] E. A. Cepeda, U. Iriarte-Velasco, B. Calvo, I. Sierra, *J. Am. Oil. Chem. Soc.,* **2016**, 93, 731–741.

Cu-$LaCoO_3$催化剂选择氢解生物质基糠醇制备1,5-和1,2-戊二醇

高芳芳[a,b], 刘海龙[a], 胡　勋[a], 陈　静[a,#], 黄志威[a,*], 夏春谷[a]
[a]中国科学院兰州化学物理研究所, 羰基合成与选择氧化国家重点实验室, 苏州研究院, 甘肃兰州730000
[b]中国科学院大学, 北京100049

摘要: 高效转化可再生生物质资源制备人类社会必需的燃料和化学品是当前关注和研究的热点之一. 生物质基糠醇来源于玉米芯、甘蔗渣、秸秆等农林副产物, 价廉易得, 是选择氢解合成高附加值1,2-和1,5-戊二醇的理想原料. 目前生物质基呋喃衍生物氢解制备二元醇的研究主要集中在Pt, Ru, Rh和Ir等贵金属催化剂, 对无Cr非贵金属催化剂的研究甚少. 基于纳米Cu催化剂较高的C–O键氢解活性和较低的C–C键裂解活性, 以及碱性载体对反应物和反应中间体的稳定作用, 我们在前期Cu-$Mg_3AlO_{4.5}$和Cu-Al_2O_3催化剂催化糠醇氢解研究基础上, 以具有一定碱性的ABO_3结构的钙钛矿型化合物为载体负载活性Cu开展糠醇氢解研究, 深入研究催化剂结构、组成和活性金属价态等对催化剂活性和选择性影响, 并研究了催化剂循环使用稳定性.

首先我们采用柠檬酸一步络合法制备了一系列具有一定钙钛矿结构的不同Cu负载量(0–20 wt%)的Cu-$LaCoO_3$催化剂以及$LaCoO_3$负载的5 wt% Pt, Ru, Rh和Pd催化剂并考察了它们的糠醇选择氢解制备戊二醇性能. 研究发现, 在相同活性金属负载量(5 wt%)时, Cu-$LaCoO_3$催化剂具有较优异的呋喃环C–O键氢解活性, 而贵金属催化剂倾向于催化呋喃环C=C键加氢饱和. 考察不同Cu负载量的Cu-$LaCoO_3$催化剂催化糠醇氢解性能发现, 随着Cu负载量的增加, 糠醇转化率先升高后降低, 在10 wt% Cu负载量时达最高(94.6%), 戊二醇总选择性也随Cu负载量的增加先升高后降低, 在5 wt% Cu负载量时最高(52.2%), 总体以10 wt% Cu负载量催化剂表现出最优异的性能.

接着我们考察了反应动力学条件如温度、压力和反应时间以及还原处理条件对10 wt%Cu-$LaCoO_3$催化性能的影响. 研究发现适当的高温(~433 K)和高压(6 MPa H_2)有利于Cu-$LaCoO_3$催化糠醇氢解制戊二醇, 而低浓度氢气(5 vol%)还原有利于1,5-戊二醇的生成, 高氢气浓度(纯氢)还原有利于呋喃环加氢饱和的四氢糠醇生成. 10 wt% Cu负载量的催化剂经5%H_2-95%N_2处理后, 在413 K和6 MPa H_2条件下可取得100%的糠醇转化率以及55.5%的戊二醇总选择性 (其中1,5-戊二醇和1,2-戊二醇的选择性之比接近3:1). 进一步考察了10 wt%Cu-$LaCoO_3$催化剂的循环使用稳定性, 研究发现无论是在高初始转化率(~93.7%)还是低初始转化率(~30.5%)条件下, 经多次循环使用后糠醇转化率先升高后基本保持不变, 而戊二醇总选择性呈下降趋势, 四氢糠醇的选择性逐渐上升.

结合XRD, XPS, BET, H_2-TPR, CO_2-TPD, NH_3-TPD和HRTEM等多种表征技术对Cu-$LaCoO_3$催化剂的结构及在糠醇氢解反应中的活性位进行了表征, 发现高分散的活性物种、合适的碱性以及部分还原的活性组分均有利于提高催化剂的活性与1,5-戊二醇的化学选择性, 高分散的Cu^0与部分还原的Co_3O_4(很可能是CoO)之间的协同催化对于取得较优异的糠醇氢解

性能, 尤其是较高的1,5-/1,2-戊二醇比例至关重要.

关键词: 糠醇; 选择性氢解; 戊二醇; 铜-钴酸镧催化剂; 钙钛矿结构

收稿日期: 2018-04-07. 接受日期: 2018-05-25. 出版日期: 2018-10-05.

*通讯联系人. 电话: (0931)4968070; 传真: (0931)4968129; 电子信箱: zwhuang@licp.cas.cn

#通讯联系人. 电话: (0931)4968068; 传真: (0931)4968129; 电子信箱: chenj@licp.cas.cn

基金来源: 国家自然科学基金(21473224); 中科院前沿科学重点研究项目(QYZDJ-SSW-SLH051); 中科院青年创新促进会(2016371); 苏州科技发展计划(SYG201626).

本文的电子版全文由Elsevier出版社在ScienceDirect上出版(http://www.sciencedirect.com/science/journal/18722067).